Seminar Indirect

Bouke Jung, Iris de Ruiter, Paul Hofland

June 2018

Contents

1 General introduction

To be written...

2 Gamma-ray experiments

2.1 Introduction

One of the ways to indirectly detect dark matter particles is to look for the gamma-ray signature of their annihilation. Two dark matter particles can annihilate to two standard model particles which then decay and leave a distinct signature in gamma-rays. Using gamma-ray telescopes that point to different regions of the sky with different optimal energy ranges, we can probe the dark matter content within the local universe. Gamma-rays are extremely powerful in creating a dark matter density map of the Universe since they are not deflected by magnetic fields, contrary to e.g. cosmic rays.
In section 2.2 we will discuss how the expected gamma-ray flux depends on the dark matter cross section and mass. Comparing the corresponding formulae to observations, it is possible to set an upper limit to the dark matter mass and cross section by the absence of an annihilation signal. In section 2.3 different complications in translating observation data to actual dark matter densities are discussed. Furthermore some typical examples of dark matter density profiles are explained. Finally in section 2.4 the current and future gamma-ray telescopes, and their efforts on constraining the dark matter parameters, are discussed.

2.2 Gamma-ray flux from dark matter WIMP annihilation - (Paul Hofland)

Nowadays, it is commonly believed that most of the universe is made out of non-baryonic cold dark matter, which consist of Weakly Interacting Massive Particles (WIMPS). The most popular WIMP candidate still remains the neutralino, as predicted by the supersymmetric extension of the standard model (SUSY). These particles are often in the GeV-TeV energy range and could be measured with two distinct methods; Direct and Indirect (note that no dark matter signal has been detected so far, but certain candidates have been either constrained or excluded [1]). The Direct measurement method looks for interactions between WIMPS and ordinary baryonic particles (such as Ge, NaI, Xe, CaF_2 molecules [2]), whereas the Indirect method looks for either gamma-rays, positions, antiprotons or neutrinos as signature. These particles are produced indirectly by pairs of WIMPs annihilations at dark matter halo locations in the galaxy. Although direct $\gamma\gamma$ or $Z\gamma$ annihilation lines are in theory possible, they are loop-suppressed. Therefore, most of the gamma-rays will follow the annihilation of pairs of quarks, leptons or Higgs bosons. The methods are complementary to each other. However, uncertain astrophysical background sources can create issues for the latter method.

In this review, we will consider neutral WIMPs that only interact trough gravitational force and annihilate into Standard Model particles via weak interactions, causing a gamma-ray to be produced indirectly as well. The energy and angle dependent gamma-ray brightness is given by formula 1:

$$I_\gamma(E,\Theta)\& = \frac{1}{2}\frac{\langle\sigma v\rangle}{m_{DM}^2}\frac{dN_{\gamma,ann}}{dE_\gamma}\frac{1}{4\pi}\int dl\rho_{DM}^2(r[l,\Theta]) \tag{1}$$

where the first half of equation 1 depends on the particle physics model of dark matter (i.e. particle physics) and the second half on the dark matter distribution (i.e. astrophysics).

2.2.1 Particle physics factor

The velocity-averaged dark matter pair annihilation cross section $\langle\sigma v\rangle$ can be estimated by looking at the relic abundance observed today due to freeze-out and linking this to the pair annihilation rate of dark matter, which implies $\langle\sigma v\rangle \sim 3\times10^{-26}cm^3s^{-1}$, see formula 4 ([3].

$$\Omega_{DM}h^2 \sim \frac{3\times10^{-27}cm^3s^{-1}}{\langle\sigma v\rangle} \tag{2}$$

The differential spectrum of emitted gamma-rays per annihilation, $\frac{dN_{\gamma,ann}}{dE_\gamma}$, can be seen as the total sum (weighted by branching ratio, see formula 5) of all spectra final states, see figure 1. Since the branching ratio and final states are very model dependent, there are major uncertainties involved in trying to explain all observable dark matter using a single WIMP dark matter candidate.

$$\frac{dN_{\gamma,ann}}{dE_\gamma} = \sum_i B_i \frac{dN^i_{\gamma,ann}}{dE_\gamma} \tag{3}$$

Where B_i is the model depended branching ratio, and $\frac{dN^i_{\gamma,ann}}{dE_\gamma}$ the individual final state spectra.

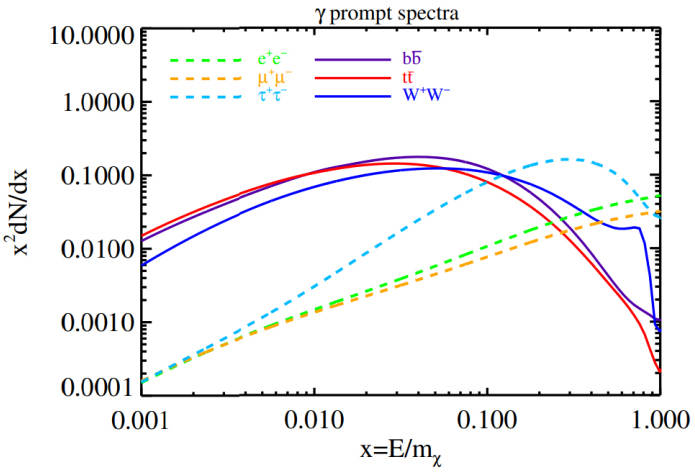

Figure 1: Figure from [3]: Gamma-ray spectrum from dark matter ($m_{DM} = 500GeV$) annihilation to six different final states, calculated using PPPC4DMID [4]

The gamma-ray brightness also contains a factor $\frac{1}{2}$, which implies that dark matter is its own anti-particle, this would be a factor $\frac{1}{4}$ otherwise. And lastly dividing by m^2_{DM} cancels out the density squared integral from the astronomical factor.

2.2.2 Astrophysical factor

The second half of the gamma-ray brightness (formula 1), consist only of the so called J-factor, which describes the amount and distribution of dark matter in a particular source. More exact; it is the line of sight integral over the dark matter density squared (ρ^2_{DM}) at an angle from the line of sight, see formula 4 for its definition.

$$J = \frac{1}{\Delta\Omega} \int \int_{\Delta\Omega} \rho^2_{DM}(l, \Omega) dl d\Omega \tag{4}$$

Note that in formula 1, the factor $\frac{1}{4\pi}$ is a normalization factor that comes from integrating over solid angle, see formula 5.

$$\int d\Omega = \int_0^{2\pi} \int_0^{\pi} \sin\theta d\theta d\phi = 4\pi \tag{5}$$

Normally, the dark matter density function (ρ_{DM}) is model based and only has an r dependence (i.e. the radial distance to the center of the dark matter source). This will be explained in greater detail in chapter 2.3. To compute the line of sight integral, we first need to relate r to l and Θ (see figure 2 for clarity).

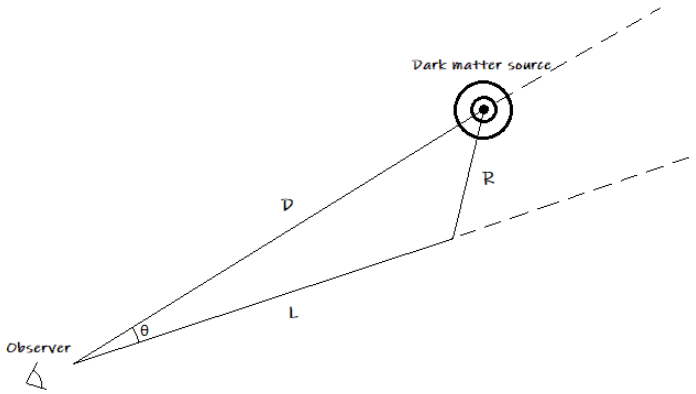

Figure 2: Top down view of observer looking down the line of sight with some angular separation Θ at a dark matter source.

Using D to denote the distance to the dark matter source and writing L for the line of sight, R for shortest distance from the line of sight to the center of the source and Θ for the angular separation of the source, we can relate R to L and Θ using the cosine rule to get formula 6.

$$R = \sqrt{L^2 + D^2 - 2L\cos\Theta} \tag{6}$$

Looking back at the total gamma-ray brightness (formula 1) and comparing this to the annihilation rate per volume, see formula 7. It becomes clear that formula 1 is just the annihilation rate per volume times the total differential spectrum of emitted gamma-rays integrated over some volume.

$$\text{Rate of annihilation per volume: } \frac{1}{2}\frac{\langle\sigma v\rangle\rho_{DM}^2}{m_{DM}^2} \tag{7}$$

2.2.3 Sagittarius gamma-ray flux

To conclude this section we show an example of a computed gamma-ray flux spectrum as a function of dark matter mass (m_χ) per annihilation channel for dwarf galaxy Sagittarius [5] (see figure 3).

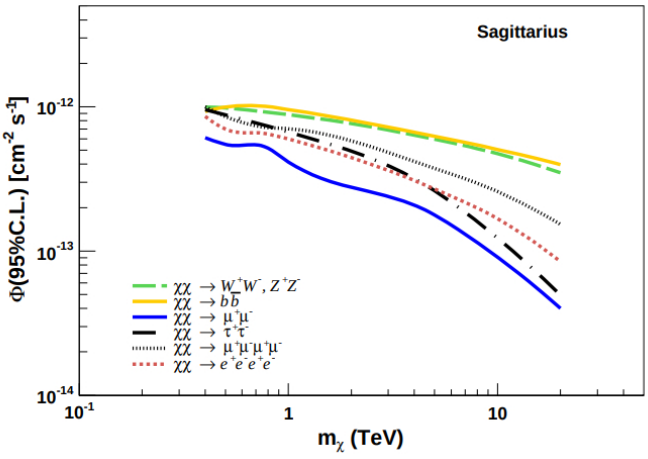

Figure 3: Figure from [5]: Gamma-ray flux as a function of dark matter mass (m_χ) under different annihilation channels.

Note that the gamma-ray flux scales with $1/m_{DM}^2$, and therefore scales down exponentially with mass. In other words; higher WIMP mass means less annihilation processes per dark matter source and therefore less gamma-rays.

2.3 Probing Dark Matter Distributions - Bouke Jung

Having discussed the theoretical background of indirect dark matter signals, the natural question arises how these signals actually manifest in the observable universe. A proper answer can only be provided in the context of the distribution of dark matter within the local universe. After all, one expects to observe a brighter gamma-ray signal in regions with high dark matter density.
Over the past decades great effort has been made to model and constrain the distribution of dark matter within the Milky Way and surrounding astrophysical objects. A few examples of recent findings are given by the discovery that the Milky Way does not conform to density profiles created from adiabatic compression [6] and the fact that neighbouring dwarf galaxies seem to exhibit dark matter distributions which become constant towards their galactic center [7]. Perhaps even more groundbreaking was the work of Diemand et al. (2008), who found evidence for the fact that dark matter can cluster together locally, forming complicated substructures which boost gamma-ray production by over an order of magnitude and cosmic ray production by a typical factor of 1.4 [8].

In this section we'll summarize some of the most prevalent models used in the context of indirect dark matter studies. Before explaining the various parameters and equations involved, however, we will first take another look at the relation between observed gamma-ray spectra and underlying dark matter distributions, in an attempt to form a better understanding of the difficulties involved with inferring flux rates from certain dark matter density profiles and vice versa.

2.3.1 Translating observational data to DM densities

The gamma-ray fluxes detected at observatories such as Fermi-LAT and the future CTA in principle contain all the information one needs in order to map dark matter distributions across galactic planes and large scale structures. As we've seen in section 2.2, there exists a direct theoretical correspondence between a source's gamma-ray intensity and the line-of-sight integral over the dark matter density. However, this is not the whole story. In making a direct comparison between the line-of-sight integral and observational fluxes, we implicitly neglect several processes of radiative transfer which could have lead to redistribution of initial dark matter generated gamma-ray fluxes — not to mention the fact that some gamma-ray detections could be misinterpreted as indirect dark matter signals, having a completely different origin all the while! Hence, in order to derive accurate conclusions regarding dark matter distributions via gamma-ray fluxes, we first have to discuss radiative transfer effects. Additionally we have to exclude the possibility of misinterpreting background signals.

Once a gamma-ray has been created through dark matter annihilation or decay, several processes might occur to it which alter the gamma-ray's energy before it reaches an observatory. Most prominent are perhaps compton scattering and pair production. In the latter case, particle-antiparticle pairs (usually electrons and positrons) are formed out of two photons. A quick order-of-magnitude calculation reveals that if the dark-matter-induced gamma-ray would undergo such a process together with a typical 2.7 Kelvin photon of the comsic microwave background (CMB) (i.e. $k_B \cdot T \approx 8.6 \cdot 2.7 \approx 10^{-4} eV$) whilst traveling through the interstellar medium, it would need to have an energy of at least $E_{\gamma,1} \cdot E_{\gamma,2} \approx E_{\gamma,1} \cdot 6.6 \cdot 10^{-4} eV \approx m_e^2 \approx 2.5 \cdot 10^{11} eV^2$. Hence, the photon initially created from dark matter annihilation or decay, would be required to have an energy greater than a few hundred TeV. For space-based gamma-ray observatories such as Fermi-LAT, which generally operate at energies of a few hundred MeV to several hundred GeV, this process should therefore not constitute any impairment in detecting dark-matter-induced gamma-rays. The upcoming Cherenkov Telescope Array (CTA) which is planned to operate between a few hundred GeV and a few hundred TeV, might have

to take the process into account.
Compton scattering may form a problem when the produced gamma-rays travel through areas in interstellar space with high electron densities. Typically, however, induced effects will not be very dramatic. Taking a characteristic electron density of a few particles per cubic centimetre and assuming that the Thomson approximation holds[1] we see that the optical depth associated with Compton scattering for a source at a distance of a few kpc would be:

$$\tau \approx n_e \sigma_T h d \approx 1\,\mathrm{cm}^{-3} \cdot 1 \times 10^{-24}\,\mathrm{cm}^2 \cdot 1 \times 10^{22}\,\mathrm{cm} \approx 10^{-5}$$

Hence we can conclude that galaxies are typically very optically thin when it comes to compton scattering. This allows one to largely ignore such processes in studying indirect dark matter signals, provided that the gamma-rays one observes did not have to propagate through any dense interstellar regions.

2.3.2 Dark matter distribution profiles

Provided that any ambiguities in ones signal have been thoroughly discussed and ruled out, it is in principle possible to construct dark matter density profiles for astrophysical objects using formula 2.2. Usually, however, researchers take the density profile as an input parameter and try to reproduce observed emission spectra numerically for comparison purposes. Over the years, a variety of different models have come into use [3]. The most recognizable one is perhaps the *Navarro-Frenk-White* (NFW) profile:

$$\rho_{NFW} = \frac{\rho_0}{\left(\frac{r}{r_s}\right)\left[1+\left(\frac{r}{r_s}\right)\right]^2} \tag{8}$$

where r denotes the distance from the center of the galactic halo and r_s is a scale radius, indicatiing the point where the logarithmic derivative of the radial density profile becomes equal to -2. In the case of the Milky Way, Fornasa and Green (2014) [9] established that $r_s \approx 20\,\mathrm{kpc}$, resulting in a dark matter density at the sun's position of around $0.4\,\mathrm{GeV/cm}^3$ and Pato et al. (2015)
Some slightly more involved profiles try to account for various deviations that cannot be modeled accurately by a pure NFW denisty profile. Particularly they create steeper profiles at the inner edges of the dark matter halo, since mechanisms involving (gravitational) interactions between dark matter and baryonic matter such as adiabatic contraction are expected to yield more concentrated dark matter distributions towards the galactic center [10, 11, 12]. Generalizing equation 2.3.2 and allowing for an arbitrary inner slope γ, we get the formula:

$$\rho_{GNFW} = \frac{\rho_0}{\left(\frac{r}{r_s}\right)^{\gamma}\left[1+\left(\frac{r}{r_s}\right)\right]^{3-\gamma}} \tag{9}$$

which reverts back to equation 2.3.2 for $\gamma = 1$. Observationally, we typically find that $0 \leq \gamma \leq 1.5$, where $\gamma = 0$ corresponds to a so-called *coned* profile, whilst $\gamma = 1.5$ is also refered to as a Moore profile [13, 14].

Contrary to the above two profiles, more recent simulations seem to suggest that galactic dark matter density profiles deviate from simple power-law dependencies, displaying slopes that vary with

[1] To be precise one would need to input the Klein-Nishina cross section for this scattering process. However, since the Thomson cross section is always bigger, we can use $\sigma_T h$ instead to retrieve an upper limit.

radius instead [15, 16, 17]. One of the first attempts at modeling such irregularity was made by *Einasto* [18], who used the formula:

$$\rho_{Ein}(r) = \rho_0 \exp -\frac{2}{a}\left[\left(\frac{r}{r_s}\right)^a - 1\right] \tag{10}$$

Observations for the Milky Way yield values around 0.2 for the parameter α.

One last dark matter density profile that we'll have to discuss is provided by *the Burkert profile*:

$$\rho_{Burk}(r) = \frac{\rho_0}{\left(1+\frac{r}{r_s}\right)\left(1+\left(\frac{r}{r_s}\right)^2\right)} \tag{11}$$

This model distinguishes itself from the rest, because it quickly flattens towards the galactic core. Since many dwarf-galaxies display density profiles which strongly deviate from power-law distributions, the Burkert formula is used very frequently in the context of these objects. Considering that spheroidal dwarf galaxies generally consist of a very low density, homogeneously distributed gas, it should come as no surprise that their (dark) matter density becomes nearly constant towards the center.

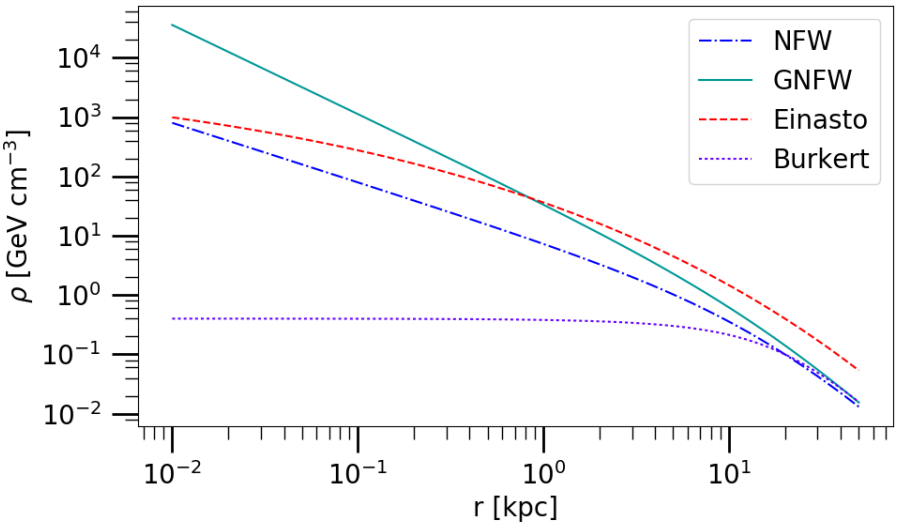

Figure 4: A graph of the various dark matter density profiles discussed within section 2.3.2. All profiles are generated using an input density $\rho_0 = 0.4$ and a scale radius $r_s = 20\,\text{kpc}$. Additionally, the GNFW spectrum was given an index $\gamma = 1.5$, whilst the Einasto spectrum received an index $a = 0.2$.

Figure 4 displays the various dark matter density profiles discussed within this section in a single panel. The differences between each of the profiles is clearly visible. The GNFW profile is the steepest and leads to large densities at the galactic core. Meanwhile, the Burkert density profile quickly flattens as the radius decreases, conform our expectations for an elliptic dwarf galaxy, which generally constitute relatively low mass, and homogeneous companion galaxies to a main host.

2.4 Current and future gamma-ray telescopes and their constraints on the dark matter cross-section - (Iris de Ruiter)

As said before we hope to detect dark matter particles via their annihilation signature. Two dark matter particles can annihilate to two standard model particles which then decay and leave a distinct signature in gamma-rays. Gamma-ray telescopes focus on the detection of gamma-rays from this dark matter annihilation process. This process is usually split up into multiple channels. The most important examples are $\chi\chi \rightarrow b\bar{b}$ and $\chi\chi \rightarrow \tau^+\tau^-$. The constraints given on the mass and cross section for the dark matter particle are given for each of these annihilation channels (bottom quarks and tau leptons), where the tau channel usually gives the strongest constraints. In the search for these annihilation processes most observations look directly at the dark matter halo of our Milky Way since this is one of the most dark matter dense regions (see section 2.3.1). Another way to get observations of dark matter dense regions is to observe regions around intermediate-mass black holes with masses in the range $10^2 \leq M/M_\odot \leq 10^6$, since there are enhancements (mini-spikes) of the dark matter densities around these black holes [19]. In the sections below we will discuss specific gamma-ray telescopes and their efforts in dark matter research.

2.4.1 Fermi-LAT

Most of our knowledge of gamma-ray emission from dark matter annihilation comes from the Fermi-LAT telescope. The LAT, which stands for Large Area Telescope, is the primary instrument on the Fermi Gamma-ray Space Telescope mission. It has a wide field-of-view for high-energy gamma-rays and it covers the range from below 20 MeV to more than 300 GeV [20]. The Fermi-LAT telescope is able to directly detect the gamma-ray emission via pair production. Observation of the Milky Way halo with Fermi-LAT provided some of the strongest constraints on the mass and cross section of the dark matter particles in the past [21].
Nowadays the best results come from the observation of dwarf spheroidal satellite galaxies (dSphs) of the Milky Way, which are some of the most dark matter dominated objects known. The lack of detection of gamma-rays gives us an upper limit to the dark matter cross section. Section 2.2 explains how the flux is related to the cross section. The newest Fermi-LAT data provide some of the most robust constraints on the dark matter mass.

For the $b\bar{b}$ annihilation channel they find $m_{DM} \gtrapprox 1$ TeV and the dark matter cross section $\langle\sigma v\rangle \lessapprox 1 \cdot 10^{-26} cm^3 s^{-1}$, for the $\tau\tau$ channel they find $m_{DM} \gtrapprox 70$ GeV and the dark matter cross section $\langle\sigma v\rangle \lessapprox 4 \cdot 10^{-26} cm^3 s^{-1}$ [22]. The results are summarized in figure 5, where the confidence intervals in the mass - cross section plane are shown for the two annihilation channels. The constraints from this publication take into account the uncertainty in the dark matter distribution of the dSphs. The Fermi-LAT telescope will be able to further constraint the mass and cross section by observing the dSphs in longer observation runs and the discovery of new dSphs.

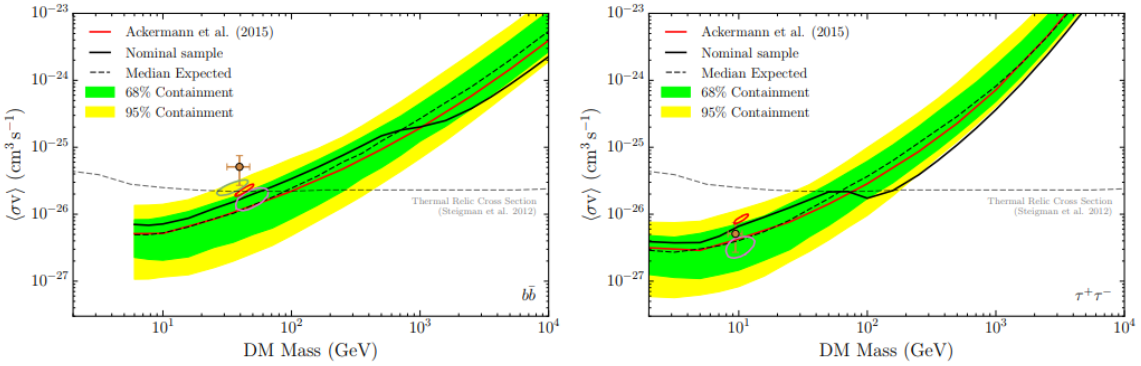

Figure 5: Figure from [22]: Constraints on the DM annihilation cross section at 95% CL for the $\chi\chi \to b\bar{b}$ (left) and $\chi\chi \to \tau^+\tau^-$ (right) channels derived from a combined analysis of 15 dSphs. Bands for the expected sensitivity are calculated by repeating the same analysis on 300 randomly selected sets of high-Galactic-latitude blank fields in the LAT data. The dashed line shows the median expected sensitivity while the bands represent the 68% and 95% quantiles. The solid black line shows the observed limit from the combined analysis of 15 dSphs from [23].The dashed gray curve in this figure corresponds to the thermal relic cross section from [24].

2.4.2 H.E.S.S.

Another important gamma-ray telescope is the H.E.S.S., which is an acronym for the High Energy Stereoscopic system. As opposed to the Fermi-LAT this is a ground based Imaging Atmospheric Cherenkov Telescope, which allows for much larger telescopes but also causes interference of the atmosphere with the gamma-ray detections. The H.E.S.S. collaboration shows a great evolution for constraints on the dark matter parameters over time. One of the first papers from 2006 concluded that there was no significant gamma-ray excess in the galactic center of the Milky Way [25]. In a 2011 publication they exclude cross sections larger than $\langle\sigma v\rangle = 3 \cdot 10^{-25} cm^3 s^{-1}$ for a dark matter mass of $m_{DM} \sim 1$ TeV [26]. The latest H.E.S.S. publication gives the strongest constraint on the dark matter cross section in for a $m_{DM} \sim 1$ TeV so far. The upper limit is given to be $\langle\sigma v\rangle = 4 \cdot 10^{-28} cm^3 s^{-1}$ [27].

2.4.3 VERITAS, MAGIC and HAWC

Other gamma-ray telescopes are also able to place constraints on the dark matter cross section, but these are usually less constrictive then the Fermi-LAT and the H.E.S.S. limits. VERITAS and MAGIC are both Imaging Atmospheric Cherenkov Telescope similar to H.E.S.S. but smaller in size. The HAWC is the High Altitude Water Cherenkov telescope, which uses water tanks to detect Cherenkov light from incoming gamma-rays as opposed to the atmosphere like H.E.S.S., VERITAS and MAGIC. The advantage of this technique is the ability to continuously run measurements at a wider field of view, instead of only at night (darkness is needed of atmospheric Cherenkov imaging).

The latest VERITAS papers constrain the cross section for the bottom quark channel to $\langle\sigma v\rangle = 1.35 \cdot 10^{-23} cm^3 s^{-1}$ and for the tau lepton channel to $\langle\sigma v\rangle = 1.32 \cdot 10^{-25} cm^3 s^{-1}$ at $m_{DM} \sim 1$ TeV [28]. As said before the recent constraints from the H.E.S.S. collaboration are about 10^{-3} times more rigid. The MAGIC collaboration finds a strongest constraint in the tau lepton annihilation channel as well: $\langle\sigma v\rangle = 3.8 \cdot 10^{-24} cm^3 s^{-1}$ at $m_{DM} \sim 0.5$ TeV [29]. Finally there is HAWC which only started observing recently and therefore has not produced constraints nearly as strong as other telescopes yet [30].

2.4.4 Future telescopes

In the near future the Cherenkov Telescope Array (CTA) hopes to improve the current limits set by H.E.S.S [32]. The CTA experiment will be the largest Imaging Atmospheric Cherenkov Telescope, taking into account telescope arrays in the northern and southern hemisphere. Since these telescopes vary in size, the CTA will improve sensitivity over a large energy range. They will be able to constraint the dark matter cross sections for dark matter masses ranging from 100 GeV to tens of TeV, with a sensitivity improved by a factor of 5-10 [32]. Fig. 6 shows how the CTA will hope to improve the dark matter cross section over a wide energy range. The sensitivity is shown in comparison with the strongest Fermi-LAT and H.E.S.S. constraints.

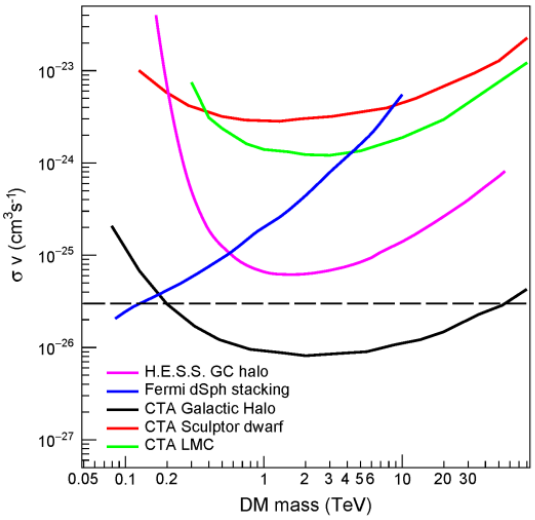

Figure 6: Figure from [31]: comparison of predicted sensitivities in for the targets of: the Milky Way Galactic halo; the Large Magellanic Cloud (LMC) and the dwarf galaxy Sculptor. The CTA sensitivity curves use the same method and W^+W annihilation modes for each target and the Einasto dark matter profile. The sensitivities for the three targets are all for 500 hours taking into account the statistical errors only.

Other planned gamma-ray telescope arrays include the CALET, GAMMA-400 and HERD. The first two telescopes have been launched recently and will improve the current resolution in small energy ranges [33, 34]. They will however not be able to improve the limits on the continuous spectrum, as set by Fermi-LAT. The HERD telescope is set to launch in 2020, and will be the most sensitive gamma-ray telescope in the 10 GeV to 1 TeV range [35]. At higher energies the Cherenkov telescopes will do better, since they have a larger effective area.

2.4.5 Comparison of gamma-ray telescopes

Table 1 shows a comparison of the discussed current (top) and future (bottom) gamma-ray telescopes in energy range, field of view, constraints on dark matter masses and cross sections.

Table 1: Comparison of different current (top) and future (bottom) gamma-ray telescopes in energy range, field of view, constraints on dark matter masses and cross sections. The right column shows the references for these parameters. *: $\frac{2}{3}$ of the sky, **:geometric factor $> 3m^2$ sr

Name	Energy range	Field of view (°)	m_{DM}	σv (cm^3/s)	Ref
Fermi-LAT	20 MeV - 300 GeV	4.2	$\sim$ 10 GeV	$\sim 4 \cdot 10^{-26}$	[20], [22]
H.E.S.S	300 GeV - 70 TeV	3.5	$\sim$ 1 TeV	$4 \cdot 10^{-28}$	[27]
Veritas	85 GeV - 30 TeV	3.5	$\sim$ 1 TeV	$2.85 \cdot 10^{-24}$	[28]
Magic	100 GeV - 100 TeV	3.5	$\sim$ 0.5 TeV	$3.8 \cdot 10^{-24}$	[29]
HAWC	500 GeV - 100 TeV	*	$\sim$ 1 TeV	$\sim 10^{-24}$	[30]
CTA	100 GeV - 10 TeV	4-5	$\sim$ 1 TeV	$5 \cdot 10^{-27} - 3 \cdot 10^{-26}$	[31], [32]
CALET	100 GeV - 1 TeV	45-58	—	—	[33]
GAMMA400	20 MeV - 1 TeV	60	—	—	[34]
HERD	10 GeV - 1 TeV	**	10 GeV 1 TeV	$6 \cdot 10^{-30} - 5 \cdot 10^{-29}$ $4 \cdot 10^{-27} - 9 \cdot 10^{-27}$	[35]

References

[1] T. M. Nieuwenhuizen. Subjecting dark matter candidates to the cluster test. *ArXiv e-prints*, October 2017.

[2] A. Bottino, V. de Alfaro, N. Fornengo, G. Mignola, and S. Scopel. On the neutralino as dark matter candidate. II. Direct detection. *Astroparticle Physics*, 2:77–90, February 1994.

[3] Jennifer M. Gaskins. A review of indirect searches for particle dark matter. *Contemporary Physics*, 57(4):496–525, 2016.

[4] Marco Cirelli, Gennaro Corcella, Andi Hektor, Gert Hütsi, Mario Kadastik, Paolo Panci, Martti Raidal, Filippo Sala, and Alessandro Strumia. Pppc 4 dm id: a poor particle physicist cookbook for dark matter indirect detection. *Journal of Cosmology and Astroparticle Physics*, 2011(03):051, 2011.

[5] A. Abramowski, F. Aharonian, F. Ait Benkhali, A. G. Akhperjanian, E. Angüner, M. Backes, S. Balenderan, A. Balzer, A. Barnacka, Y. Becherini, and et al. Search for dark matter annihilation signatures in H.E.S.S. observations of dwarf spheroidal galaxies. , 90(11):112012, December 2014.

[6] Fabio Iocco, Miguel Pato, Gianfranco Bertone, and Philippe Jetzer. Dark matter distribution in the milky way: microlensing and dynamical constraints. *Journal of Cosmology and Astroparticle Physics*, 2011(11):029, 2011.

[7] Frank C. van den Bosch and Rob A. Swaters. Dwarf galaxy rotation curves and the core problem of dark matter haloes. *Monthly Notices of the Royal Astronomical Society*, 325(3):1017–1038, 2001.

[8] J. Diemand, M. Kuhlen, P. Madau, M. Zemp, B. Moore, D. Potter, and J. Stadel. Clumps and streams in the local dark matter distribution. , 454:735–738, August 2008.

[9] Mattia Fornasa and Anne M Green. Self-consistent phase-space distribution function for the anisotropic dark matter halo of the milky way. *Physical Review D*, 89(6):063531, 2014.

[10] Paolo Gondolo and Joseph Silk. Dark matter annihilation at the galactic center. *Physical Review Letters*, 83(9):1719, 1999.

[11] Oleg Y Gnedin, Andrey V Kravtsov, Anatoly A Klypin, and Daisuke Nagai. Response of dark matter halos to condensation of baryons: cosmological simulations and improved adiabatic contraction model. *The Astrophysical Journal*, 616(1):16, 2004.

[12] Oleg Y Gnedin, Daniel Ceverino, Nickolay Y Gnedin, Anatoly A Klypin, Andrey V Kravtsov, Robyn Levine, Daisuke Nagai, and Gustavo Yepes. Halo contraction effect in hydrodynamic simulations of galaxy formation. *arXiv preprint arXiv:1108.5736*, 2011.

[13] B. Moore, T. Quinn, F. Governato, J. Stadel, and G. Lake. Cold collapse and the core catastrophe. , 310:1147–1152, December 1999.

[14] J. J. Adams, J. D. Simon, M. H. Fabricius, R. C. E. van den Bosch, J. C. Barentine, R. Bender, K. Gebhardt, G. J. Hill, J. D. Murphy, R. A. Swaters, J. Thomas, and G. van de Ven. Dwarf Galaxy Dark Matter Density Profiles Inferred from Stellar and Gas Kinematics. , 789:63, July 2014.

[15] J. F. Navarro, E. Hayashi, C. Power, A. R. Jenkins, C. S. Frenk, S. D. M. White, V. Springel, J. Stadel, and T. R. Quinn. The inner structure of ΛCDM haloes - III. Universality and asymptotic slopes. , 349:1039–1051, April 2004.

[16] Liang Gao, Julio F Navarro, Shaun Cole, Carlos S Frenk, Simon DM White, Volker Springel, Adrian Jenkins, and Angelo F Neto. The redshift dependence of the structure of massive λ cold dark matter haloes. *Monthly Notices of the Royal Astronomical Society*, 387(2):536–544, 2008.

[17] J. F. Navarro, A. Ludlow, V. Springel, J. Wang, M. Vogelsberger, S. D. M. White, A. Jenkins, C. S. Frenk, and A. Helmi. The diversity and similarity of simulated cold dark matter haloes. , 402:21–34, February 2010.

[18] J. Einasto. On the Construction of a Composite Model for the Galaxy and on the Determination of the System of Galactic Parameters. *Trudy Astrofizicheskogo Instituta Alma-Ata*, 5:87–100, 1965.

[19] Gianfranco Bertone, Andrew R Zentner, and Joseph Silk. New signature of dark matter annihilations: Gamma rays from intermediate-mass black holes. *Physical Review D*, 72(10):103517, 2005.

[20] WB Atwood, Aous A Abdo, Markus Ackermann, W Althouse, B Anderson, M Axelsson, L Baldini, J Ballet, DL Band, Guido Barbiellini, et al. The large area telescope on the fermi gamma-ray space telescope mission. *The Astrophysical Journal*, 697(2):1071, 2009.

[21] Markus Ackermann, Marco Ajello, WB Atwood, Luca Baldini, Guido Barbiellini, D Bastieri, K Bechtol, R Bellazzini, RD Blandford, ED Bloom, et al. Constraints on the galactic halo dark matter from fermi-lat diffuse measurements. *The Astrophysical Journal*, 761(2):91, 2012.

[22] Andrea Albert, Brandon Anderson, Keith Bechtol, Alex Drlica-Wagner, Manuel Meyer, Miguel Sánchez-Conde, L Strigari, M Wood, TMC Abbott, Filipe B Abdalla, et al. Searching for dark matter annihilation in recently discovered milky way satellites with fermi-lat. *The Astrophysical Journal*, 834(2):110, 2017.

[23] M Ackermann, A Albert, Brandon Anderson, WB Atwood, L Baldini, G Barbiellini, D Bastieri, K Bechtol, R Bellazzini, E Bissaldi, et al. Searching for dark matter annihilation from milky way dwarf spheroidal galaxies with six years of fermi large area telescope data. *Physical Review Letters*, 115(23):231301, 2015.

[24] Gary Steigman, Basudeb Dasgupta, and John F Beacom. Precise relic wimp abundance and its impact on searches for dark matter annihilation. *Physical Review D*, 86(2):023506, 2012.

[25] Felix Aharonian, AG Akhperjanian, AR Bazer-Bachi, M Beilicke, Wystan Benbow, David Berge, K Bernlöhr, C Boisson, Oliver Bolz, V Borrel, et al. Hess observations of the galactic center region and their possible dark matter interpretation. *Physical Review Letters*, 97(22):221102, 2006.

[26] A Abramowski, Fabio Acero, F Aharonian, AG Akhperjanian, G Anton, A Barnacka, U Barres De Almeida, AR Bazer-Bachi, Yvonne Becherini, J Becker, et al. Search for a dark matter annihilation signal from the galactic center halo with hess. *Physical Review Letters*, 106(16):161301, 2011.

[27] H. Abdallah et al. Search for γ-Ray Line Signals from Dark Matter Annihilations in the Inner Galactic Halo from 10 Years of Observations with H.E.S.S. *Phys. Rev. Lett.*, 120(20):201101, 2018.

[28] S Archambault, A Archer, W Benbow, R Bird, E Bourbeau, T Brantseg, M Buchovecky, JH Buckley, V Bugaev, K Byrum, et al. Dark matter constraints from a joint analysis of dwarf spheroidal galaxy observations with veritas. *Physical Review D*, 95(8):082001, 2017.

[29] Max L Ahnen, S Ansoldi, LA Antonelli, C Arcaro, D Baack, A Babić, B Banerjee, P Bangale, U Barres de Almeida, JA Barrio, et al. Indirect dark matter searches in the dwarf satellite galaxy ursa major ii with the magic telescopes. *Journal of Cosmology and Astroparticle Physics*, 2018(03):009, 2018.

[30] AU Abeysekara, A Albert, R Alfaro, C Alvarez, R Arceo, JC Arteaga-Velázquez, D Avila Rojas, HA Ayala Solares, A Becerril, E Belmont-Moreno, et al. A search for dark matter in the galactic halo with hawc. *Journal of Cosmology and Astroparticle Physics*, 2018(02):049, 2018.

[31] The Cherenkov Telescope Array Consortium, BS Acharya, I Agudo, I Al Samarai, R Alfaro, J Alfaro, C Alispach, R Alves Batista, J-P Amans, E Amato, et al. Science with the cherenkov telescope array. *arXiv preprint arXiv:1709.07997*, 2017.

[32] The CTA Consortium. Design concepts for the cherenkov telescope array. *arXiv preprint arXiv:1008.3703*, 2010.

[33] O Adriani, Y Akaike, K Asano, Y Asaoka, MG Bagliesi, G Bigongiari, WR Binns, S Bonechi, M Bongi, JH Buckley, et al. The calorimetric electron telescope (calet) for high-energy astroparticle physics on the international space station. In *Journal of Physics: Conference Series*, volume 632, page 012023. IOP Publishing, 2015.

[34] NP Topchiev, AM Galper, V Bonvicini, O Adriani, RL Aptekar, IV Arkhangelskaja, AI Arkhangelskiy, AV Bakaldin, L Bergstrom, E Berti, et al. Gamma-400 gamma-ray observatory. *arXiv preprint arXiv:1507.06246*, 2015.

[35] Xiaoyuan Huang, Anna S Lamperstorfer, Yue-Lin Sming Tsai, Ming Xu, Qiang Yuan, Jin Chang, Yong-Wei Dong, Bing-Liang Hu, Jun-Guang Lü, Le Wang, et al. Perspective of monochromatic gamma-ray line detection with the high energy cosmic-radiation detection (herd) facility onboard china's space station. *Astroparticle Physics*, 78:35–42, 2016.

2.5 Review papers

https://arxiv.org/pdf/1707.06277.pdf WIMP dark matter candidates and searches – current status and future prospects

Indirect detection of dark matter - Lars Bergstrom (2007)

J. M. Gaskins, A review of indirect searches for particle dark matter, Contemp. Phys. (2016) https://arxiv.org/pdf/1604.00014.pdf

Indirect detection of dark matter - J. Carr et al. (2006)

Ackerman et al. (2015) ; "*Searching for Dark Matter Annihilation from Milky Way Dwarf Spheroidal Galaxies with Six Years of Fermi Large Area Telescope Data*"

2.6 Scale Radii

M. A. Breddels and A. Helmi, "Model comparison of the dark matter profiles of Fornax, Sculptor, Carina and Sextans", A&A 559, 10 p., (2013) https://arxiv.org/pdf/1304.2976.pdf

2.7 ID DM signal radiative transfer

Profumo, S. and Jeltema, E.T. (2011) ; *"Extragalactic Inverse Compton Light from Dark Matter annihilation and the Pamela positron excess"* http://iopscience.iop.org/article/10.1088/1475-7516/2009/07/020/meta